Journal of Power Sources 185 (2008) 807–814

Contents lists available at ScienceDirect

Journal of Power Sources

journal homepage: www.elsevier.com/locate/jpowsour

Nanoparticles of Pt/H_xMoO_3 electrodeposited in poly (3,4-ethylenedioxythiophene)-poly(styrene sulfonic acid) as the electrocatalyst for methanol oxidation

Chung-Wen Kuo[a], Chinnaiah Sivakumar[b], Ten-Chin Wen[a,*]

[a] Department of Chemical Engineering, National Cheng Kung University, Tainan 70101, Taiwan
[b] Electrodics & Electrocatalysis Division, Central Electrochemical Research Institute, Karaikudi 630006, Tamil Nadu, India

ARTICLE INFO

Article history:
Received 23 May 2008
Received in revised form 11 July 2008
Accepted 15 July 2008
Available online 30 July 2008

Keywords:
Pt/H_xMoO_3
PEDOT-PSS
XPS
SEM
Methanol oxidation

ABSTRACT

Nanoparticles of platinum and hydrous molybdenum oxide (Pt/H_xMoO_3) were successfully electrodeposited onto poly(3,4-ethylenedioxythiophene)-poly(styrene sulfonic acid) (PEDOT-PSS) film by chronocoulometry (0.2 C). Various loadings of Pt/H_xMoO_3 particles onto the PEDOT-PSS electrode were achieved using the co-deposition technique. The existence of Pt/H_xMoO_3 particles was determined through characterization by X-ray photoelectron spectroscopy (XPS) and X-ray diffraction (XRD) analysis. XPS results revealed that deposited Pt and molybdenum were metallic Pt and H_xMoO_3, respectively. XRD analysis showed a decrease of Pt crystalline facets for the incorporation of H_xMoO_3 into PEDOT-PSS-Pt, indicating a strong interaction between Pt and H_xMoO_3. Scanning electron microscopy (SEM) results revealed a uniform dispersion of Pt/H_xMoO_3 particles, with the particle size of 70–90 nm, in the PEDOT-PSS matrix. The cyclic voltammetry study and chronopotentiometry measurements demonstrated that the PEDOT-PSS-Pt/H_xMoO_3 electrode had superior electrocatalytic activity of methanol oxidation with less CO poisoning. The presence of amorphous H_xMoO_3 particles on the Pt surface minimized CO poisoning of methanol oxidation.

1. Introduction

Direct methanol fuel cells (DMFCs) are considered a promising solution to future energy problems because of their high-energy conversion efficiency, low pollutant emission, low operating temperature, and the simplicity of handling and processing liquid fuel [1,2]. The development of DMFCs has the problem of slow methanol oxidation reaction kinetics at the Pt anode catalyst. This is mainly due to the self-poisoning of Pt surfaces caused by the adsorption of reaction intermediates CO and CO-like species [3]. A few researchers have attempted to reduce the amount of adsorbed CO on Pt surfaces by employing added metal catalysts such as Ru, Sn, W, Mo, and Os to promote CO oxidation [4–6]. Molybdenum can improve the activity of platinum toward the oxidation of methanol when it is added into platinum as an alloy element or a compound [7,8]. The mechanism of methanol oxidation on Pt in the presence of molybdenum oxide species has been reported in literature [9–12]. The Mo oxide species in Pt promote the oxidative removal of adsorbed CO intermediates. The enhancement of surface catalytic activity by Pt-Mo oxide interaction and the large surface area achieved with low loading levels improves DMFCs.

Conducting polymer matrix is a solid support alternative to carbon that can be used as a DMFC electrode catalyst because it provides uniform distribution of metal nanoparticles into the polymer matrix in a 3D manner. Pt particles dispersed in the polymer matrix (PEDOT-PSS) exhibit interesting catalytic properties [13–16] because of the large number of catalytic sites. In the past few years, several articles have been published on the electrocatalytic properties of platinum alloys such as Pt-Ru incorporated into conducting polymeric matrix [17,18]. It has been shown that a modified electrode with polymer has better catalytic performance than a modified electrode without polymer toward the oxidation of methanol. The high surface area of conducting polymers has made them popular as supporting materials in the development of new electrocatalysts [19,20]. Because of the relatively high electric conductivity of conducting polymers, it is possible to shuttle the electrons through polymer chains between the electrodes and dispersed metal particles where the electrocatalytic reaction occurs. Thus, an efficient electrocatalyst can be achieved in the composite materials.

In the present study, a composite form of conducting polymer, PEDOT-PSS, was used as a 3D-random matrix for loading Pt and

* Corresponding author. Tel.: +886 6 2385487; fax: +886 6 2344496.
E-mail address: tcwen@mail.ncku.edu.tw (T.-C. Wen).

0378-7753/$ – see front matter © 2008 Elsevier B.V. All rights reserved.
doi:10.1016/j.jpowsour.2008.07.060

H_xMoO_3 particles. PEDOT is a high surface area conducting polymer with good environmental stability, high electrical conductivity, very good film forming properties, and a high degree of doping compared to PANI and other conducting polymers [21]. It can be used as an electrode catalyst support for Pt particles for the oxidation of small organic molecules such as methanol. Ghosh and Inganas [21] reported that PEDOT-PSS is a non-stoichiometric polyelectrolyte complex of PEDOT and PSS, with an excess of the latter component. PEDOT-PSS is commercially available as stable aqueous dispersion. The network structure and SO_3^- groups of PEDOT-PSS [22] permit increased uptake of Pt^{4+} ions [13] and facilitate the uniform distribution of Pt particles in a polymer matrix. The polymer matrix is used as a protective layer to prevent nanoparticles aggregation after their formation. Since H_xMoO_3 can promote the oxidative removal of adsorbed CO intermediates on Pt surfaces [23,24], different methods of loading Pt/H_xMoO_3 particles entrapped in the PEDOT-PSS matrix are examined to find the best electrocatalytic activity and stability toward methanol oxidation.

2. Experimental

A PEDOT-PSS (Alfa, 1.34 wt%) matrix electrode was prepared by spin coating 100 μl (2 drops) of dispersion onto indium-tin oxide (ITO) substrate at 2000 rpm for 1 min. After the completion of the spin coating process, films were dried at 150 °C for 3 min. A thin film of PEDOT-PSS formed over a cleaned indium-tin oxide electrode (1.0 cm × 1.0 cm). Before each experiment, ITO coated glass was cleaned in an ultrasonic bath using detergent, double distilled water, and isopropanol, then dried with a dry nitrogen flow followed by UV-O_3 treatments for 30 min.

Pt, H_xMoO_3, and Pt/H_xMoO_3 particles were incorporated into the PEDOT-PSS film by electrochemical deposition/co-deposition from 0.01 M HCl + 0.1 M KCl solution containing 5 mM $H_2PtCl_6{\cdot}6H_2O$ (PEDOT-PSS-Pt), 1 mM $Na_2MoO_4{\cdot}2H_2O$ (PEDOT-PSS-H_xMoO_3), 5 mM $H_2PtCl_6{\cdot}6H_2O$, and 1 mM $Na_2MoO_4{\cdot}2H_2O$ (PEDOT-PSS-Pt/H_xMoO_3) at a constant potential of −0.2 V (vs. Ag/AgCl). For comparison purposes, Pt, H_xMoO_3, and Pt/H_xMoO_3 particles were also deposited on a bare ITO electrode (E-Pt, E-H_xMoO_3, and Pt/H_xMoO_3) with a process similar to the deposition of Pt, H_xMoO_3, and Pt/H_xMoO_3 particles onto PEDOT-PSS, respectively. Constant deposition charge of 0.2 C was maintained for all deposition processes, except that PEDOT-PSS-H_xMoO_3 and E-H_xMoO_3 electrodes were kept at 0.04 C. After deposition, the electrodes were rinsed with double distilled water for 5 min and then dried at 150 °C for 3 min.

Electrochemical characterizations of PEDOT-PSS-Pt, PEDOT-PSS-H_xMoO_3, and PEDOT-PSS-Pt/H_xMoO_3 composite electrodes were carried out using a PGSTAT20 electrochemical analyzer, AUTOLAB Electrochemical Instrument (The Netherlands). All experiments were performed in a three-component cell. An Ag/AgCl electrode (in 3 M KCl), Pt wire, and ITO coated glass plate (1 cm^2 area) were used as reference, counter, and working electrodes, respectively. A Luggin capillary, whose tip was set at a distance of 1–2 mm from the surface of the working electrode, was used to minimize errors due to the *iR* drop in the electrolytes. The catalytic activities of E-H_xMoO_3, E-Pt/H_xMoO_3, PEDOT-PSS-Pt, and PEDOT-PSS-Pt/H_xMoO_3 composite electrodes were examined in 0.1 M CH_3OH + 0.5 M H_2SO_4 solution at the potential range of −0.2 to 1.0 V with a scanning rate of 50 mV s^{-1}.

X-ray photoelectron spectroscopy (XPS) was performed using ESCA 210 spectrometers. XPS spectra employed Mg Kα ($h\nu$ = 1253.6 eV) irradiation as the photon source, with a primary tension of 12 kV. The pressure during the scans was approximately 10^{-10} mbar. Morphological and crystalline behavior changes among electrodes fabricated with indium-tin oxide as the substrate, and E-Pt/H_xMoO_3, PEDOT-PSS-Pt, and PEDOT-PSS-Pt/H_xMoO_3 films were compared using scanning electron microscopy (SEM) (Philips X1-40 FEG.), energy dispersive spectroscopy (EDS), and X-ray diffraction (XRD) analysis, respectively. X-ray diffraction spectra for the as-prepared electrodes were obtained by exposing the samples to a Sieman D5000 X-ray source with Cu Kα (1.542 Å) as a target in diffraction angles (2θ) ranging from 10° to 90° with a scanning rate of 4° min^{-1}. An Impedance Spectrum Analyzer, IM6 (ZAHNER, Germany), with Thales software was employed to measure and analyze the ac impedance spectra of electrodes obtained at various element resistances. The potential amplitude of ac was kept at 10 mV and a frequency range of 50 mHz to 100 kHz was used.

3. Results and discussion

Conducting PEDOT-PSS film used as a catalyst support was formed in ITO glass by the spin coating process. The PEDOT-PSS film thickness (202 nm) and electrochemical stability were measured by ellipsometry and the cyclic voltammetry (CV) technique as described elsewhere [13]. To investigate the electrocatalytic activity of Pt/H_xMoO_3 nanoparticles loaded PEDOT-PSS film, two different approaches were taken: (i) electrocodeposition of various amounts Pt/H_xMoO_3 particles onto PEDOT-PSS and (ii) electrodeposition of various amounts of H_xMoO_3 particles onto constant Pt (0.1 mg cm^{-2}) particles incorporated PEDOT-PSS film. The detailed procedure of the deposition of Pt/H_xMoO_3 particles in the PEDOT-PSS film was described in Section 2. The cyclic voltammetry technique was chosen to characterize the Pt and Pt/H_xMoO_3 particles embedded in PEDOT-PSS film in 0.5 M H_2SO_4 and compared with bare E-Pt, E-Pt/H_xMoO_3 electrodes.

3.1. Deposition of Pt and co-deposition of Pt/H_xMoO_3 particles on the PEDOT-PSS electrode

Pt and Pt/H_xMoO_3 nanoparticles were electrodeposited on PEDOT-PSS film using the chronocoulometry technique. The detailed procedure of the deposition of Pt and Pt/H_xMoO_3 particles is described in Section 2. Fig. 1 shows the typical cyclic voltammograms of Pt and Pt/H_xMoO_3 particles loaded PEDOT-PSS film in the potential range of −0.2 and 1.0 V vs. Ag/AgCl at

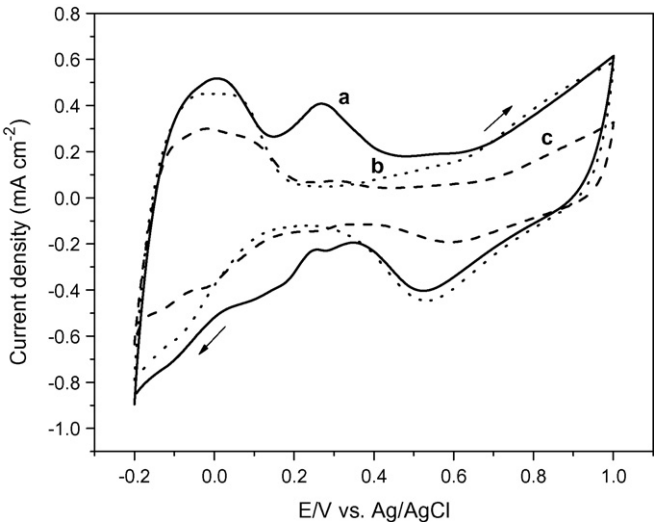

Fig. 1. Cyclic voltammograms of (a) PEDOT-PSS-Pt/H_xMoO_3 prepared using the co-deposition technique, (b) PEDOT-PSS-Pt and (c) PEDOT-PSS-Pt/H_xMoO_3 obtained by the deposition of H_xMoO_3 on PEDOT-PSS-Pt electrodes in 0.5 M H_2SO_4 with a potential range of −0.2 and 1.0 V at a scanning rate of 50 mV s^{-1}.

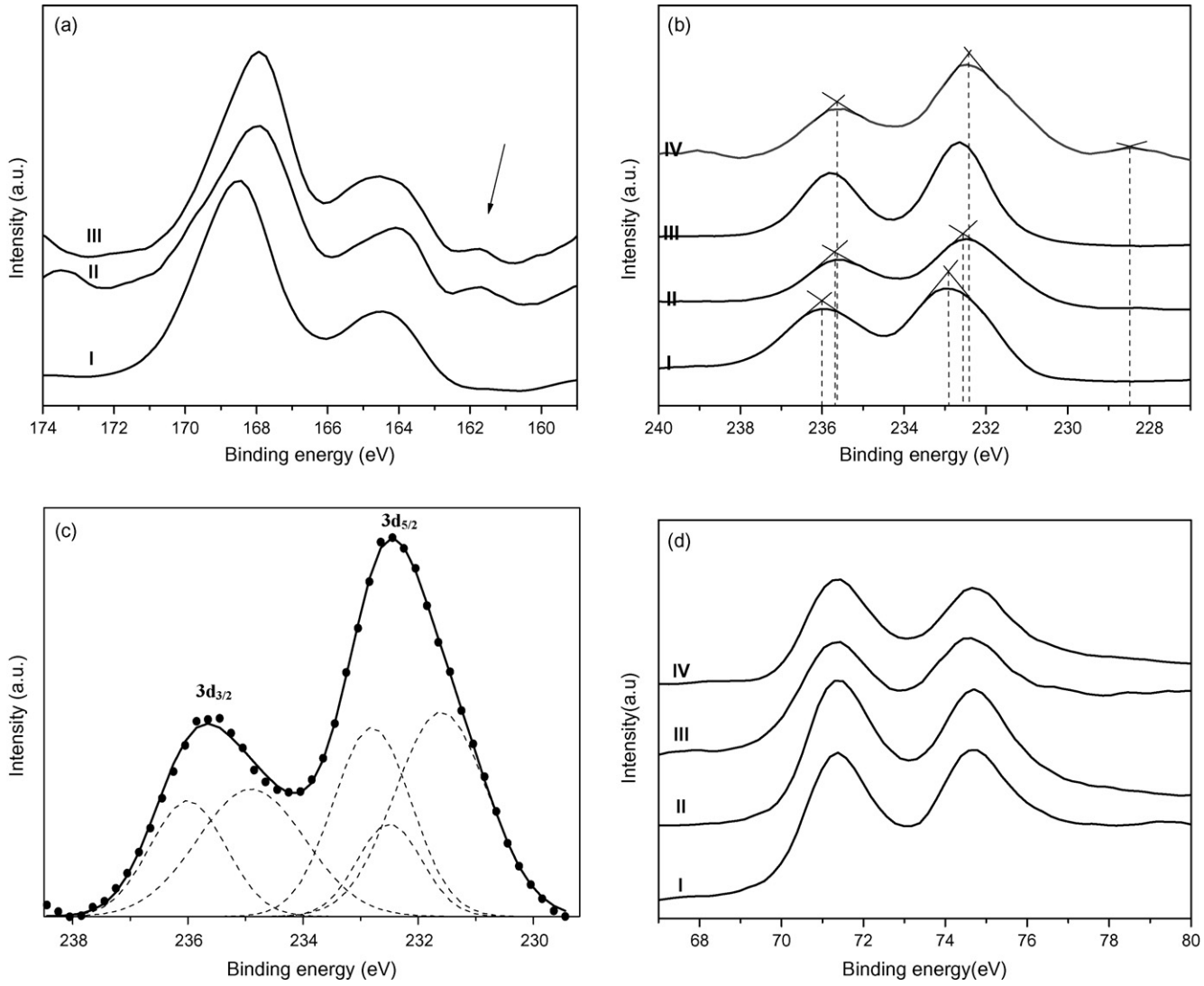

Fig. 2. (a) S 2p XPS core-level spectra of (I) PEDOT-PSS, (II) PEDOT-PSS-Pt, and (III) PEDOT-PSS-Pt/H_xMoO_3. (b) Mo 3d XPS core-level spectra of (I) E-H_xMoO_3, (II) PEDOT-PSS-H_xMoO_3, (III) E-Pt/H_xMoO_3, and (IV) PEDOT-PSS-Pt/H_xMoO_3. (c) Supplementary deconvolution of Mo 3d core level spectra of PEDOT-PSS-Pt/H_xMoO_3. (d) Pt 4f XPS core-level spectra of (I) E-Pt, (II) PEDOT-PSS-Pt, (III) E-Pt/H_xMoO_3, and (IV) PEDOT-PSS-Pt/H_xMoO_3.

a scanning rate of 50 mV s^{-1} in 0.5 M H_2SO_4. A clear skin texture of hydrogen adsorption–desorption of Pt nanoparticles with no sharp peaks was observed [20] in the potential range of −0.2 and 0.1 V, which indicates that the Pt particles were dispersed uniformly in the PEDOT-PSS 3D-random matrix (curve a). Because of the PEDOT-PSS matrix, the electrodeposited Pt and Pt/H_xMoO_3 nanoparticles have a high surface area (1.978 mC cm^{-2} for PEDOT-PSS-Pt and 3.220 mC cm^{-2} for PEDOT-PSS-Pt/H_xMoO_3) compared to Pt and Pt/H_xMoO_3 particles deposited on the bare ITO electrode (figure not shown). An additional new redox peak was observed at 0.254 V on the anode side and a broad peak at 0.282 V on the cathode side for Pt/H_xMoO_3 particle loaded PEDOT-PSS film (curve a). This indicates that the particles of H_xMoO_3 were co-deposited with Pt particles and that a trioxide of Mo exists in the redox transition between +4 and +6 states with non-stoichiometric mixed valences (H_xMoO_3/H_yMoO_3; $0 < y < x < 2$), which is similar to the hydrogen molybdenum bronze obtained by the reduction of molybdates in acid solutions [9,24,25]. A close examination of the hydrogen adsorption–desorption region of CV of PEDOT-PSS-Pt and PEDOT-PSS-Pt/H_xMoO_3 electrodes produced almost the same peak current values, indicating that the co-deposited H_xMoO_3 particles do not affect the real surface area of Pt particles in the PEDOT-PSS-Pt/H_xMoO_3 matrix. During co-deposition process, H_xMoO_3 particles are covered on the surface of Pt particles and hence aggregation of Pt particles is avoided in PEDOT catalyst support. But electrodeposition of Pt particles onto PEDOT-PSS matrix results Pt particles agglomeration. H_xMoO_3 particles may be located nearby or adjacent to Pt (1 1 1) surface of Pt particles. We observed high electro-active surface area and electrocatalytic activity of PEDOT-PSS-Pt/H_xMoO_3 catalyst toward methanol oxidation compared to the catalyst prepared by electrodeposition of Pt particles on PEDOT-PSS matrix. Hence H_xMoO_3 particles can be assisted to incorporate Pt particles in PEDOT-PSS matrix with uniform distribution and avoided particles aggregation to certain extent. However, a reduced electro-active surface of Pt particles was noticed on the Pt/MoO_x/C catalyst prepared by the impregnation of Pt particles on MoO_x/C dispersed in ethanol solution [24] compared to the PEDOT-PSS-Pt/H_xMoO_3 catalyst. To obtain the maximum loading of Pt/H_xMoO_3 particles onto PEDOT-PSS matrix, co-deposition (deposition charge = 0.2 C) of various amounts of H_xMoO_3 was performed between 0.5 mM of [Na_2MoO_4] and 3 mM of [Na_2MoO_4] with constant Pt loading [5 mM of H_2PtCl_6]

on the PEDOT-PSS electrodes. The surface area (3.220 mC cm^{-2}) of Pt/H_xMoO_3 particles loaded PEDOT-PSS film increased with increasing [Na_2MoO_4] until 1 mM of [Na_2MoO_4] was reached and then decreased.

To obtain the highest electro-active surface area of Pt/H_xMoO_3 particles loaded PEDOT-PSS film, various amounts of H_xMoO_3 with a constant Pt particles (100 μg cm^{-2}) amount loaded PEDOT-PSS electrodes were obtained by chronocoulometric deposition using a precursor salt solution of Na_2MoO_4 with the different deposition charge. A representative voltammogram is shown in Fig. 1 (curve c) for comparison. All composite electrodes of PEDOT-PSS-Pt/H_xMoO_3 had a reduced electro-active surface area (1.362 mC cm^{-2}) compared to the composite electrodes prepared using the co-deposition technique (3.220 mC cm^{-2}). The Pt surface area was almost 2.3 times smaller. This is due to the surface blocking of H_xMoO_3 particles onto the real surface area of Pt particles loaded PEDOT-PSS film. Therefore, the co-deposition technique is more effective for loading Pt/H_xMoO_3 particles into the PEDOT-PSS matrix to get a high electro-active surface area of the anode catalyst for methanol oxidation.

3.2. XPS study of Pt and Pt/H_xMoO_3 particles loaded PEDOT-PSS film

An XPS study was conducted to analyze the binding energy related to S 2p core-level spectra of PEDOT-PSS, PEDOT-PSS-Pt, and PEDOT-PSS-Pt/H_xMoO_3. The sulfur core level spectrum of PEDOT-PSS film coated on ITO is shown in Fig. 2a (curve I). The curve shows large differences in binding energy depending on the S location of PEDOT and PSS. The peak at 168.5 eV corresponds to a spin-orbit splitting doublet originating from the sulfur atoms of PSS dopants. The spin-orbit splitting doublet of PEDOT sulfur originates at 164.5 eV [26,27]. These observations are similar to the binding energy of S 2p core level spectra of PEDOT-PSS film obtained by sputtering on ITO [28]. By the addition of Pt or Pt/H_xMoO_3 nanoparticles on PEDOT-PSS film, significant changes occurred in the S 2p core value of sulfur in both PEDOT and PSS. Curves II and III show the formation of a new shoulder peak (C-S-Pt binding energy) at approximately 161.7 eV. This result is in agreement for typical C-S-metal bonds appearing in the range of 162 and 161 eV [29]. Jonsson et al. [27] reported that aluminum/PEDOT-PSS contains an interfacial layer formed by chemical interactions between aluminum and mainly sulfonic groups of poly(styrenesulfonic acid) (PSS). The sulfur atoms of PSS might bond with Pt atoms more easily than with those of PEDOT. This is due to the fact that PEDOT is doped with an excess of PSS, which can react easily with the Pt particle surface. From the analysis of S elements, we concluded that there was a strong interaction between Pt particles and sulfonic acid groups of PEDOT-PSS.

The Mo core-level spectra of E-H_xMoO_3 (H_xMoO_3 particles were deposited onto a simple ITO electrode), PEDOT-PSS-H_xMoO_3, Pt-H_xMoO_3, and PEDOT-PSS-Pt/H_xMoO_3 are shown in Fig. 2b. According to XPS data of binding energy [30], the characteristic $3d_{5/2}$ and $3d_{3/2}$ doublet peaks appear at 232.8 and 236.0 eV with a peak separation value of 3.2 eV. This is an evidence of the formation of H_xMoO_3 (Mo^{6+}) on the ITO electrode (curve I). With the co-deposition of Pt/H_xMoO_3 particles on ITO (curve III) and PEDOT-PSS (curve IV) electrodes, both peaks were shifted slightly to higher binding energy values (232.52 eV for Mo $3d_{5/2}$ and 235.65 eV for Mo $3d_{3/2}$) compared to H_xMoO_3 particles deposition on a bare ITO electrode. An additional broad binding energy peak was observed at 228.5 eV in curve IV, indicating the existence of H_xMoO_3 particles in the +4 state (Mo^{4+}). No predominant 3d spin-orbit coupling peak was observed at 227.7 eV, which corresponds to metallic Mo particles formed in the co-deposition process. Further, the Mo $3d_{3/2}$ peak of H_xMoO_3 diminished after co-deposition with Pt. The broadness of Mo $3d_{5/2}$ and $3d_{3/2}$ peaks (curve IV) indicate that the co-deposited H_xMoO_3 particles may have different valences of Mo (Mo^{6+}, Mo^{5+}, and Mo^{4+}), which is similar to the co-deposition of Pt/H_xMoO_3 particles on glassy carbon [11], H_xMoO_3 particles deposited on TiO_2 [31] electrodes, and the spontaneous spread of MoO_3 on Au (1 1 1) surfaces [32]. In order to confirm the existence of the mixed valence of H_xMoO_3 in PEDOT-PSS-Pt/H_xMoO_3 film, supplementary deconvolution of curve IV was performed. The deconvoluted spectral lines are presented in Fig. 2c. The Mo $3d_{5/2}$ and $3d_{3/2}$ binding energy peaks at 231.6 and 234.9 eV, respectively are characteristic of the Mo^{+5} state. The Mo^{+4} state of H_xMoO_3 is concluded from the 3d spin-orbit binding energy peaks at 229.3 and 232.5 eV. These observations are evidence of the formation of the redox couple of $H_xMoO_3 \rightarrow H_yMoO_3$ ($0 < y < x < 2$) in the CV of the PEDOT-PSS-Pt/H_xMoO_3 electrode. The Pt core-level spectra of E-Pt (Pt particles were deposited onto a simple ITO electrode), PEDOT-PSS-Pt, Pt/H_xMoO_3, and PEDOT-PSS-Pt/H_xMoO_3 are shown in Fig. 2d. The intensive Pt 4f binding energy peaks at 71.3 and 74.7 eV is the characteristic of metallic Pt [33]. Therefore, Pt particles were found in a zero oxidation state in the co-deposition of Pt/H_xMoO_3 on PEDOT-PSS electrode. A comparison of Pt 4f core-level spectra reveals that the spectra for E-Pt, PEDOT-PSS-Pt, Pt/H_xMoO_3, and PEDOT-PSS-Pt/H_xMoO_3 are virtually identical. Hence, the prescribed experimental conditions favor the formation of Pt/H_xMoO_3 particles in the PEDOT-PSS matrix with the co-deposition process.

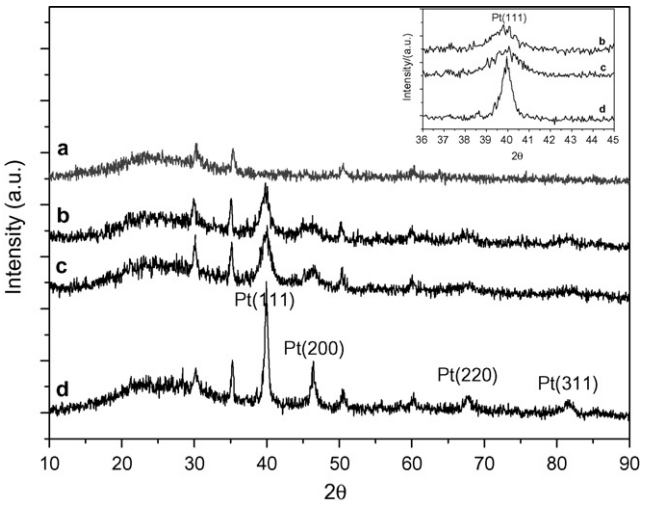

Fig. 3. XRD patterns of (a) E-ITO, (b) PEDOT-PSS-Pt/H_xMoO_3, (c) E-Pt/H_xMoO_3, and (d) PEDOT-PSS-Pt.

3.3. Structural characterization of Pt particles in the absence and presence of H_xMoO_3 in PEDOT-PSS film

The surface morphology of Pt and Pt-H_xMoO_3 particles incorporated PEDOT-PSS electrodes was examined by XRD analysis, as shown in Fig. 3. The characteristic diffraction peaks (curve a) of bare ITO were observed at about 31°, 36°, 51°, and 61°, corresponding to (2 2 2), (4 0 0), (4 4 0), and (6 2 2) planes, respectively. The XRD pattern of PEDOT-PSS-Pt obtained using the same preparation method is shown in curve d. The characteristic diffraction peaks of face centered cubic (fcc) platinum were observed at 39.95°, 46.45°, 68°, and 81°, corresponding to Pt (1 1 1), (2 0 0), (2 2 0), and (3 1 1) planes, respectively. The diffraction peaks of H_xMoO_3 were not found in the XRD pattern of PEDOT-PSS-Pt/H_xMoO_3 and Pt/H_xMoO_3 (curves b and c) due to either the amorphous structure or low-crystallinity

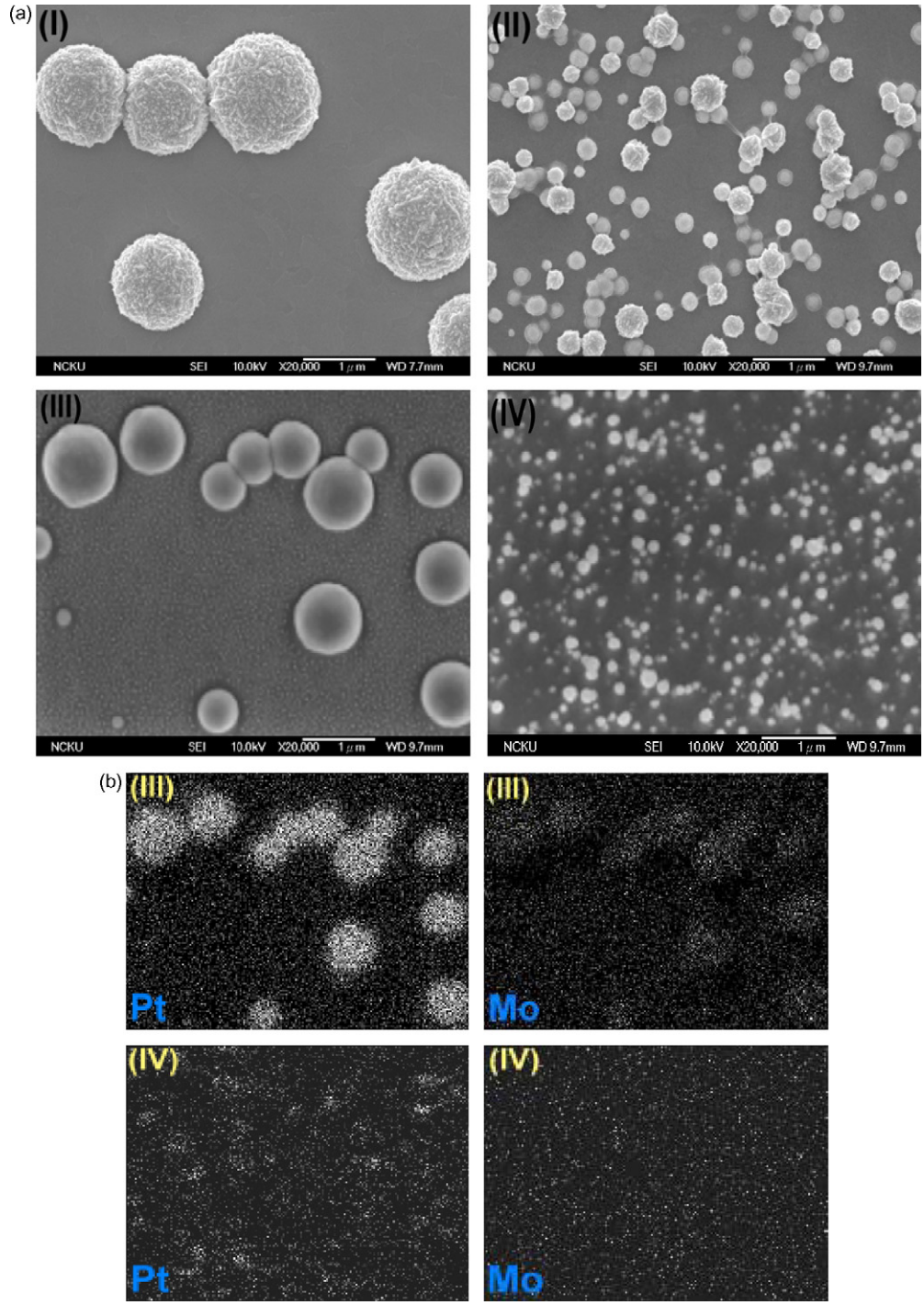

Fig. 4. (a) SEM images of (I) E-Pt, (II) PEDOT-PSS-Pt, (III) E-Pt/H_xMoO_3, and (IV) PEDOT-PSS-Pt/H_xMoO_3. (a)–(d) are magnified ×20,000. (b) EDS of Pt and Mo-mapping of E-Pt/H_xMoO_3 from Fig. 3a (III) and PEDOT-PSS-Pt/H_xMoO_3 from Fig. 3a (IV), respectively.

of H_xMoO_3 [24]. With the co-deposition of Pt/H_xMoO_3 particles onto PEDOT-PSS film, the diffraction peak values of Pt (1 1 1) and Pt (2 0 0) facets shifted to lower values (39.28° and 45.93°) compared to the respective Pt facets in bare ITO. The Pt (1 1 1) and Pt (2 0 0) facets of PEDOT-PSS-Pt/H_xMoO_3 become broader than PEDOT-PSS-Pt, which indicates the dispersing nature of Pt nanoparticles with less particles aggregation in the PEDOT matrix. This is clearly shown in the inset of Fig. 3. The reduced peak intensity of Pt (1 1 1) and Pt (2 0 0) facets was also observed for both PEDOT-PSS-Pt/H_xMoO_3 and Pt/H_xMoO_3, indicating that the crystalline lattice of platinum might be influenced by the existence of H_xMoO_3 particles in composite systems and that a strong interaction exists between Pt and H_xMoO_3.

3.4. Surface morphology of Pt, Pt/H_xMoO_3 particles in ITO and PEDOT-PSS film

Fig. 4a and b shows the scanning electron microscopy analysis of the surface morphology and particles mapping analysis of E-Pt, PEDOT-PSS-Pt, Pt/H_xMoO_3, and PEDOT-PSS-Pt/H_xMoO_3 electrodes.

The aggregation of Pt particles is clearly shown on bare ITO for the simple deposition of Pt (picture I)). Smaller Pt particles (100–200 nm) with a high active surface area were observed for PEDOT-PSS-Pt electrode compared to E-Pt. Since PEDOT-PSS acts as a 3D-random matrix, SO_3^- groups of PEDOT-PSS absorb Pt^{4+} ions and a protective layer to prevent the aggregation of Pt nanoparticles after Pt formation. The S 2p core level spectra of XPS shows that the PEDOT-PSS-Pt electrode has a strong interaction between platinum and sulfonic groups of PEDOT-PSS. Homogeneous distribution of Pt/H_xMoO_3 particles can be clearly seen in the PEDOT-PSS-Pt/H_xMoO_3 matrix with an average particles size of 50–70 nm after the co-deposition of metal precursor salt solution using the chronocoulometry technique. In contrast to E-Pt and PEDOT-PSS-Pt, less aggregation of Pt particles can be observed for Pt/H_xMoO_3 and PEDOT-PSS-Pt/H_xMoO_3. A possible explanation is that the addition of H_xMoO_3 might inhibit the agglomeration of Pt particles [34]. H_xMoO_3 was not observed for all composite electrodes in the SEM images. Hence, particles mapping analysis was conducted to understand their surface morphology. Fig. 4b shows the Pt and Mo-mapping of E-Pt/H_xMoO_3 and PEDOT-PSS-Pt/H_xMoO_3 electrodes. The bright spots represent Pt and Mo elements. The density of H_xMoO_3 bright spots in E-Pt/H_xMoO_3 is higher than that of in PEDOT-PSS-Pt/H_xMoO_3 on access to Pt position. This illustrates that the interaction between Pt and H_xMoO_3 particles is strong after the co-deposition of Pt/H_xMoO_3 in the PEDOT-PSS matrix, which further supports the XRD results.

3.5. Electrocatalytic activity of Pt, H_xMoO_3, and Pt/H_xMoO_3 particles loaded on ITO and PEDOT-PSS film

Pt, H_xMoO_3, and Pt/H_xMoO_3, particles were loaded onto bare ITO, and PEDOT-PSS composite electrodes and tested for their electrocatalytic activity of methanol oxidation by cyclic voltammetry. Fig. 5a shows the voltammograms of E-H_xMoO_3, PEDOT-PSS-Pt, and PEDOT-PSS-Pt/H_xMoO_3 composite electrodes in 0.5 M H_2SO_4 solution containing 0.1 M methanol at a scanning rate of 50 mV s^{-1}. Comparing the CV results of the three electrodes, a significantly higher oxidation current toward methanol oxidation was observed for PEDOT-PSS-Pt/H_xMoO_3. A maximum anodic peak current density of 2.220 mA cm^{-2} was observed for PEDOT-PSS-Pt/H_xMoO_3 electrode at 0.8 V (compared with PEDOT-PSS-Pt (1.540 mA cm^{-2})). The enhanced catalytic activity of PEDOT-PSS-Pt/H_xMoO_3 toward methanol oxidation is attributed to the easy oxidation of methanol due to the existence of H_xMoO_3 particles in PEDOT-PSS-Pt. PEDOT could not be a poison to Pt. The interaction between PEDOT and Pt is less than that between Pt and methanol. The mechanism has been proposed for the oxidation of methanol in 0.5 M H_2SO_4 at the PEDOT-Pt electrode by the dissociative adsorption process. This renders a series of adsorbed intermediates formed on the Pt surface. PEDOT is not only nonpoisonous to Pt surface but also reduces CO poison to Pt. The high current density observed in this study is a result of less CO poisoning of Pt particles due to the fast reaction between H_xMoO_3 particles and Pt-CO intermediates at lower potentials during methanol oxidation compared with the C-Pt/Ru standard catalyst. In addition, PEDOT-PSS film is a good 3D polymer matrix, allowing maximum utilization of methanol molecules on the surface of Pt/H_xMoO_3 particles. The onset of methanol oxidation occurs at about 0.45, 0.51, and 0.54 V for PEDOT-PSS-Pt/H_xMoO_3, Pt/H_xMoO_3, and PEDOT-PSS-Pt, respectively, indicating that PEDOT-PSS-Pt/H_xMoO_3 has superior electrocatalytic performance for methanol oxidation. However, the voltammograms of E-H_xMoO_3 and PEDOT-PSS-H_xMoO_3 electrodes show that no characteristic methanol oxidation peak was present in 0.5 M H_2SO_4 solution containing 0.1 M of methanol, indicating that H_xMoO_3 particles are electro-catalytically inactive toward methanol oxidation. Hence, the PEDOT-PSS-Pt/H_xMoO_3 electrode showed an enhanced electrocatalytic activity and is an alternative anode catalyst for the oxidation of small organic molecules like methanol.

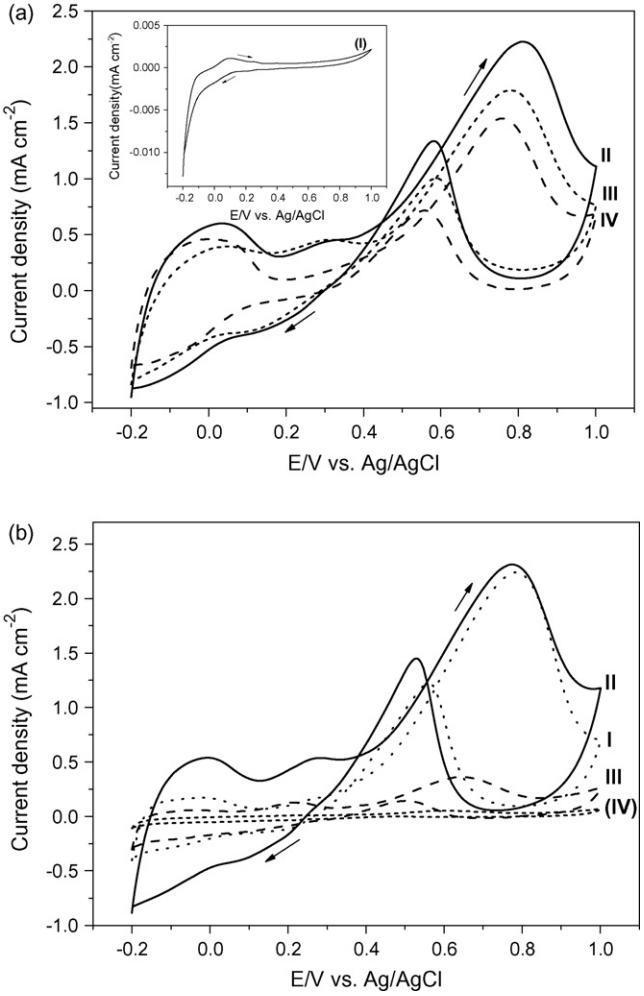

Fig. 5. Cyclic voltammogram of (a) (I) E-H_xMoO_3 (inset), (II) PEDOT-PSS-Pt/H_xMoO_3, (III) E-Pt/H_xMoO_3, and (IV) PEDOT-PSS-Pt electrodes. (b) Co-deposition (0.2 C) of various amounts of H_xMoO_3 with constant Pt loading on PEDOT-PSS electrodes (I) 0.5 mM Na_2MoO_4 + 5 mM H_2PtCl_6, (II) 1 mM Na_2MoO_4 + 5 mM H_2PtCl_6, (III) 2 mM Na_2MoO_4 + 5 mM H_2PtCl_6, and (IV) 3 mM Na_2MoO_4 + 5 mM H_2PtCl_6 recorded for 0.1 M CH_3OH oxidation in a potential range of −0.2 and 1.0 V with a scanning rate of 50 mV s^{-1} in 0.5 M H_2SO_4.

Fig. 5b shows the voltammograms recorded for 0.1 M methanol oxidation of various amounts of Pt/H_xMoO_3 particles loaded onto PEDOT-PSS by the co-deposition method in 0.5 M H_2SO_4 at a scanning rate of 50 mV s^{-1}. By varying [Na_2MoO_4] at a fixed Pt precursor (5 mM of H_2PtCl_6), an increase in peak current density of methanol oxidation was observed until 1 mM of Na_2MoO_4 was reached (curve II). After a further increase of the Mo precursor, a decrease in trend of methanol oxidation was observed which indicates that the electro-active surface area of Pt particles was blocked by excess H_xMoO_3.

The PEDOT-PSS-Pt/H_xMoO_3 electrode (Fig. 1, curve a) has a higher electro-active surface area (1.64 times) than that of PEDOT-PSS-Pt with the same deposition charge (0.2 C). This is due to the homogenous distribution of Pt particles with less aggregation after co-deposition with H_xMoO_3 particles. The redox couple of H_xMoO_3 particles appeared at lower potentials (approximately 0.254 V vs.

Ag/AgCl) with +4 and +5 transition states and was strong enough to interact with Pt particles before methanol oxidation started. The existence of H_xMoO_3 particles in the polymer matrix is highly favored by the presence of PSS in the PEDOT matrix. The free sulfonic acid group of PSS provides protons to H_xMoO_3 when it loses protons. Hence, the formation of molybdenum trioxide (MoO_3) can be prevented in the PEDOT-PSS matrix and H_xMoO_3 ($0 < x < 2$) can be kept constant during the methanol oxidation process on the Pt surface [35]. Fuel cell performances as a function of time of operation of up to 70 h for the composite membrane. Polystyrene sulfonate (PSS) membranes have high proton conductivity and low cost, but it has low tensile modulus and is susceptible to chemical degradation in the oxidizing environment of the fuel cell [36]. But, PEDOT-PSS polymer is a 3D-network polymer structure, lower water swelling property, and increases the membrane resistance time. Hence PEDOT-PSS polymer may have slow rate of membrane degradation than PSS membrane.

The following mechanism has been proposed for the oxidation of methanol in 0.5 M H_2SO_4 at the PEDOT-PSS-Pt/H_xMoO_3 electrode by the dissociative adsorption process. This results in a series of adsorbed intermediates forming on the Pt surface [36,37].

$$CH_3OH + Pt \rightarrow Pt\text{-}(CH_ZO)_{ad} + (4-Z)H^+ + (4-Z)e^- \quad (0 \le Z \le 4) \tag{1}$$

$$Pt\text{-}H_yMoO_3 + H_2O \rightarrow Pt\text{-}H_xMoO_3(OH) \quad (\textit{before the onset of methanol oxidation})$$

The role of H_xMoO_3 particles in platinum-H_xMoO_3 catalysts for methanol oxidation is similar to that of ruthenium in platinum-ruthenium catalysts [38], in which species on ruthenium can oxidize the adsorption of CO on platinum [39]. H_xMoO_3 helps the transformation of adsorbed intermediates to carbon dioxide. The clean Pt surface then becomes available for further oxidation of methanol.

$$Pt\text{-}(CH_ZO)_{ad} + Pt\text{-}H_yMoO_3 + H_2O \rightarrow Pt + Pt\text{-}H_xMoO_3 + CO_2 \tag{2}$$

$$Pt\text{-}H_xMoO_3 \rightarrow Pt\text{-}H_yMoO_3 + (x-y)e^- + (x-y)H^+$$

3.6. Chronopotentiometric study of the PEDOT-PSS-Pt/H_xMoO_3 electrode

The chronopotentiometry technique was used to study the anti-poisoning effect of catalysts toward methanol oxidation [40,41]. The electrode potentials of all the catalysts increased gradually for several minutes and then jumped to higher potentials (Fig. 6). A possible explanation is as follows [41]: during the chronopotentiometric experiment, CO accumulates on the surface of platinum particles and reduces the electrocatalytic activity of the catalysts. When the electrocatalysts are poisoned, the methanol oxidation reaction cannot continue. The onset potential of methanol oxidation was observed at about 0.47, 0.49, and 0.52 V for PEDOT-PSS-Pt/H_xMoO_3, Pt/H_xMoO_3 and PEDOT-PSS-Pt electrodes, respectively.

The time (T) at which the electrode potential jumps to a higher potential is introduced to examine the anti-poisoning ability of the catalyst. The T value of PEDOT-PSS-Pt/H_xMoO_3 (T = 52 min) is higher than that (T = 2 min) of PEDOT-PSS-Pt due to the existence of H_xMoO_3. This can be explained by the fact that the H_xMoO_3 particles embedded on the PEDOT-Pt surface enhance the oxidation of adsorbed CO molecules to CO_2. The T value of PEDOT-PSS-Pt/H_xMoO_3 is higher than that (T = 44 min) of the Pt/H_xMoO_3 electrode. Here, the PEDOT matrix may influence the electro-oxidation

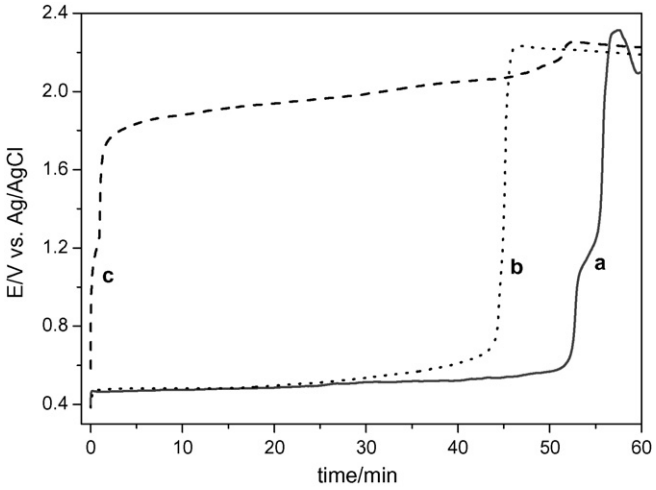

Fig. 6. Chronopotentiometric curves of (a) PEDOT-PSS-Pt/H_xMoO_3, (b) E-Pt/H_xMoO_3, and (c) PEDOT-PSS-Pt electrodes in 0.1 M CH_3OH + 0.5 M H_2SO_4 solution at a constant current of 0.3 mA cm^{-2}.

of small organic molecules [42]. The polymer may: (1) hinder the formation of strongly absorbed poisonous species; (2) catalyze the oxidation of strongly adsorbed poisonous species; and (3) catalyze the oxidation of weekly adsorbed poisonous species. The poisoning effect may be restricted in the presence of H_xMoO_3 and PEDOT-PSS. These results show that the PEDOT-PSS-Pt/H_xMoO_3 catalyst has better anti-poisoning ability, which is important for fuel cells, than that of the reported PANI-Pt/H_xMoO_3 [35].

3.7. Electrochemical impedance spectroscopy measurements

Electrochemical impedance spectroscopy (EIS) was used to determine the charge-transfer resistance of PEDOT-PSS-Pt, Pt-H_xMoO_3, and PEDOT-PSS-Pt/H_xMoO_3 electrodes toward methanol oxidation. Fig. 7 shows the Nyquist plots obtained in 0.1 M CH_3OH + 0.5 M H_2SO_4 solution at an applied potential of 0.40 V vs. Ag/AgCl with an ac amplitude of 10.0 mV for PEDOT-PSS-Pt, Pt/H_xMoO_3, and PEDOT-PSS-Pt/H_xMoO_3 electrodes. At 0.40 V, CO

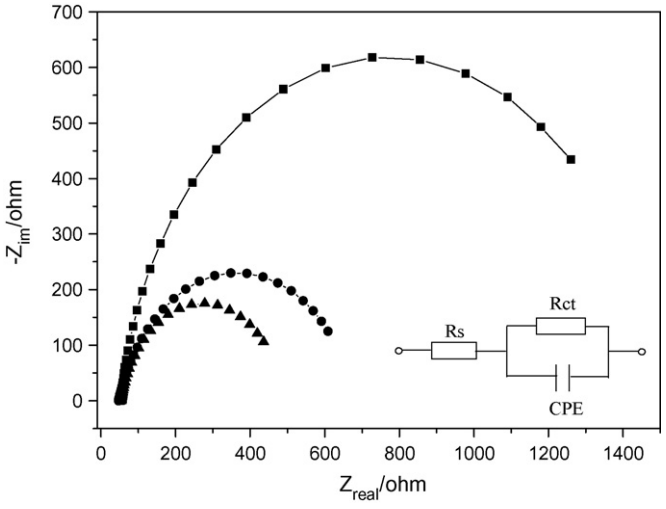

Fig. 7. Nyquist plots for PEDOT-PSS-Pt (■), E-Pt/H_xMoO_3 (●), and PEDOT-PSS-Pt/H_xMoO_3 (▲) electrodes in 0.1 M CH_3OH + 0.5 M H_2SO_4 solution and an applied potential of 0.40 V vs. Ag/AgCl using an ac amplitude of 10.0 mV. Equivalent circuit used to fit the impedance spectra (inset).

was absorbed on the surface of platinum particles during the methanol oxidation process and H_xMoO_3 appears in the higher oxidation state, which can oxidize CO molecules adsorbed on the surface of platinum particles. To interpret the impedance results, an equivalent circuit was used to fit the EIS data in Fig. 7 (inset). In this Rs(RctCPE) circuit, Rs represents ohmic resistance of the solution, while RctCPE represents the parallel combination of the charge-transfer resistance (Rct) and the constant phase element (CPE). The parallel combination (Rct and CPE) leads to a depressed semicircle in the corresponding Nyquist impedance plot.

According to experiment data based on the equivalent circuit, it is clear that the lowest charge-transfer resistance (Rct = 438 Ω) can be observed for PEDOT-PSS-Pt/H_xMoO_3 than PEDOT-PSS-Pt (Rct = 1439 Ω) due to the presence of H_xMoO_3 in the PEDOT-PSS matrix. This can be explained by H_xMoO_3 oxidizing the CO on the platinum surface to form CO_2. The charge-transfer resistance of PEDOT-PSS-Pt/H_xMoO_3 is lower than that of Pt-H_xMoO_3 (Rct = 637 Ω). This means that the embedding of Pt/H_xMoO_3 nanoparticles inside the PEDOT-PSS matrix may lead to a faster charge transfer in the parallel PEDOT-PSS film/solution and Pt/H_xMoO_3/solution interface than in the Pt/H_xMoO_3(microparticles)/solution. The PEDOT-PSS matrix may also hinder the formation of strongly absorbed poisonous species.

4. Conclusion

A high electro-active surface area (3.220 mC cm^{-2}) of Pt/H_xMoO_3 particles was successfully electrodeposited into the PEDOT-PSS matrix for methanol oxidation. The existence of H_xMoO_3 particles in PEDOT-PSS-Pt/H_xMoO_3 was verified using cyclic voltammetry. The $3d_{5/2}$ and $3d_{3/2}$ core level spectra of Mo further support the existence of H_xMoO_3. XPS of S elements analyzed that PEDOT-PSS-Pt indicates a strong interaction between platinum and sulfonic groups of PEDOT-PSS. XRD results further confirmed that the crystalline lattice of platinum might be influenced by the existence of amorphous H_xMoO_3 in composite systems. The composite PEDOT-PSS-Pt/H_xMoO_3 based electrode proved to be a promising catalyst for methanol oxidation. The PEDOT-PSS-Pt/H_xMoO_3 electrode exhibits a high current density (2.220 mA cm^{-2}) and a low onset potential toward methanol oxidation. The PEDOT-PSS matrix provides an environment for dispersing Pt particles with less aggregation, which is evident from SEM results. H_xMoO_3 favors the transformation of CO to carbon dioxide on the platinum surface. A clean Pt surface then becomes available for the oxidation of methanol. The enhanced electrocatalytic activity of Pt in PEDOT-PSS might allow a decrease in the use of Pt content in DMFCs applications.

Acknowledgement

The financial support of this work by the National Science Council of Taiwan under grants NSC-95-221-E-006-325, NSC-95-2811-E-006-021, NSC-95-ET-7-006-006-ET, and NSC-95-2211-E-006-409-MY3 is gratefully acknowledged.

References

[1] A.S. Arico, S. Srinivasan, V. Antonucci, Fuel Cells 1 (2001) 133.
[2] K.Y. Chan, J. Ding, J. Ren, S. Cheng, K.Y. Tsang, J. Mater. Chem. 14 (2004) 505.
[3] W. Vielstich, J. Braz. Chem. Soc. 14 (2003) 503.
[4] N.M. Markovic, H.A. Gasteiger, C.A. Lucas, I.M. Tidswell, P.N. Ross, Electrochim. Acta 40 (1995) 91.
[5] G. Wu, L. Li, B.Q. Xu, Electrochim. Acta 50 (2004) 1.
[6] M.J. Gonzalez, C.H. Peters, M.S. Wrighton, J. Phys. Chem. B 105 (2001) 5470.
[7] H. Massong, H. Wang, G. Samjeske, H. Baltruschat, Electrochim. Acta 46 (2000) 701.
[8] W.S. Li, L.P. Tian, Q.M. Huang, H. Li, H.Y. Chen, X.P. Lian, J. Power Sources 104 (2002) 281.
[9] J.A. Shropshire, J. Electrochem. Soc. 112 (1965) 465.
[10] J. Lu, W.S. Li, J.H. Du, J.M. Fu, J. New Mater. Electrochem. Syst. 8 (2005) 5.
[11] Y. Wang, E.R. Fachini, G. Cruz, Y. Zhu, Y. Ishikawa, J.A. Colucci, C.R. Cabrera, J. Electrochem. Soc. 148 (2001) C222.
[12] S. Mukerjee, R.C. Urian, Electrochim. Acta 47 (2002) 3219.
[13] C.W. Kuo, L.M. Huang, T.C. Wen, A. Gopalan, J. Power Sources 160 (2006) 65.
[14] N. Toshima, Y. Shiraishi, T. Teranishi, M. Miyake, T. Tominaga, H. Watanabe, W. Brijoux, H. Bonnemann, G. Schmid, Appl. Organomet. Chem. 15 (2001) 178.
[15] M. Lin, W. Yu, H. Lin, T. Zheng, J. Colloid Interface Sci. 214 (1999) 231.
[16] J.-H. Choi, K.-W. Park, H.-K. Lee, Y.-M. Kim, J.-S. Lee, Y.-E. Sung, Electrochim. Acta 48 (2003) 2781.
[17] S. Kim, S.J. Park, Solid State Ionics 178 (2008) 1915.
[18] A.N. Golikand, S.M. Golabi, M.G. Maragheh, L. Irannejad, J. Power Sources 145 (2005) 116.
[19] A. Malinauskas, Synth. Met. 107 (1999) 75.
[20] C. Sivakumar, Electrochim. Acta 52 (2007) 4182.
[21] S. Ghosh, O. Inganas, Adv. Mater. 11 (1999) 1214.
[22] F. Blanchard, B. Carre, F. Bonhomme, P. Biensan, H. Pages, D. Lemordant, J. Electroanal. Chem. 569 (2004) 203.
[23] E.I. Santiago, G.A. Camara, E.A. Ticianelli, Electrochim. Acta 48 (2003) 3527.
[24] T. Ioroi, N. Fujiwara, Z. Siroma, K. Yasuda, Y. Miyazaki, Electrochem. Commun. 4 (2002) 442.
[25] C. Ritter, W. Muller-Warmuth, R. Schollhorm, J. Chem. Phys. 83 (1985) 6130.
[26] G. Greczynski, T. Kugler, W.R. Salaneck, Thin Solid Films 354 (1999) 129.
[27] S.K.M. Jonsson, W.R. Salaneck, M. Fahlman, J. Mater. Res. 18 (2003) 1219.
[28] J. Hwang, F. Amy, A. Kahn, Org. Electron. 7 (2006) 387.
[29] W. Deng, L. Yang, D. Fujita, H. Nejoh, C. Bai, Appl. Phys. A 71 (2000) 639.
[30] C.D. Wagner, W.M. Riggs, L.E. Davis, J.F. Moulder, G.E. Muilenberg, in: G.E. Muilenberg (Ed.), Handbook of X-ray Photoelectron Spectroscopy, Perkin-Elmer Corporation, Eden Prairie, 1979.
[31] A. Katrib, A. Benadda, J.W. Sobczak, G. Maire, Appl. Catal. A 242 (2003) 31.
[32] Z. Song, T. Cai, Z. Chang, G. Liu, J.A. Rodriguez, J. Hrbek, J. Am. Chem. Soc. 125 (2003) 8059.
[33] L. Li, H.X. Wang, B.Q. Xu, J.L. Li, T.H. Lu, Z.Q. Mao, Acta Chim. Sin. 61 (2003) 818.
[34] Y.S. Kim, H.J. Ahn, H.S. Shim, S.H. Nam, T.Y. Seong, W.B. Kim, Electrochem. Solid-State Lett. 10 (8) (2007) A180.
[35] W. Li, J. Lu, J. Du, D. Lu, H. Chen, H. Li, Y. Wu, Electrochem. Commun. 7 (2005) 406.
[36] J.F. Drillet, R. Dittmeyer, K. Juttner, L. Li, K.M. Mangold, Fuel Cells 6 (2006) 432.
[37] R. Parsons, T. Vander Noot, J. Electroanal. Chem. 257 (1988) 9.
[38] S. Mukerjee, J. Mcbreen, J. Electrochem. Soc. 146 (1999) 600.
[39] M. Watanable, S. Motoo, J. Electroanal. Chem. 60 (1975) 267.
[40] M. Krausa, W. Vielstich, J. Electroanal. Chem. 399 (1995) 7.
[41] J. Chen, M. Wang, B. Liu, Z. Fan, K. Cui, Y. Kuang, J. Phys. Chem. B 110 (2006) 11775.
[42] V.E. Kazarinov, V.N. Andreev, M.A. Spitsyn, A.P. Mayorov, Electrochim. Acta 35 (1990) 1459.